Regular Article

Magainin-H2 effects on the permeabilization and mechanical properties of giant unilamellar vesicles

Andrea Mescola[a, 1]

andrea.mescola@nano.cnr.it

Nathaly Marín-Medina[b, 1]

nmarinm@uniandes.edu.co

Gregorio Ragazzini[a, c]

gregorio.ragazzini@unimore.it

Maurizio Accolla[c]

Andrea Alessandrini[a, c, *]

andrea.alessandrini@unimore.it

[a]CNR-Nanoscience Institute-S3, Via Campi 213/A, 41125 Modena, Italy

[b]Department of Physics, University of Los Andes, Carrera 1 N° 18A – 12, Bogotá, Colombia

[c]Department of Physics, Informatics and Mathematics, University of Modena and Reggio Emilia, Via Campi 213/A, 41125 Modena, Italy

*Corresponding author at: Department of Physics, Informatics and Mathematics, University of Modena and Reggio Emilia, 41125 Modena, Italy.

[1]These two authors contributed equally to the work

Abstract

Among the potential novel therapeutics to treat bacterial infections, antimicrobial peptides (AMPs) are a very promising substitute due to their broad-spectrum activity and rapid bactericidal action. AMPs strongly interact with the bacterial membrane, and the need to have a correct understanding of the interaction between AMPs and lipid bilayers at a molecular level prompted a wealth of experimental and theoretical studies exploiting a variety of AMPs. Here, we studied the effects of magainin H2 (Mag H2), an analog of the well-known magainin 2 (*wt* Mag 2) AMP endowed with a higher degree of hydrophobicity, on giant unilamellar vesicles (GUVs) concentrating on its permeabilization activity and the effect on the lipid bilayer mechanical properties. We demonstrated that the increased hydrophobicity of Mag H2 affects its selectivity conferring a strong permeabilization activity also on zwitterionic lipid bilayers. Moreover, when lipid mixtures including PG lipids are considered, PG has a protective effect, at variance from *wt* Mag 2, suggesting that for Mag H2 the monolayer curvature could prevail over the peptide-membrane electrostatic interaction. We then mechanically characterized GUVs by measuring the effect of Mag H2 on the bending constant of lipid bilayers by flickering spectroscopy and, by using micropipette aspiration technique, we followed the steps leading to vesicle permeabilization. We found that Mag H2, notwithstanding its enhanced hydrophobicity, has a pore formation mechanism compatible with the toroidal pore model similar to that of *wt* Mag 2.

Keywords: Antimicrobial peptides; Magainin H2; Micropipette aspiration; Giant unilamellar vesicles; Flickering spectroscopy; Optical microscopy

Abbreviations: AMP, antimicrobial peptide; CF, carboxyfluorescein; CL, cardiolipin; DHPE, 1,2-dihexadecanoyl-*sn-glycero*-3-phosphoethanolamine; DOPC, 1,2-dioleoyl-*sn-glycero*-3-phosphocholine; EC_{50}, Effective concentration 50%; GUV, giant unilamellar vesicle; *wt* Mag 2, magainin 2; Mag H2, magainin H2; MAT, micropipette aspiration technique; MIC, minimum inhibitory concentration; P/L, peptide-to-lipid ratio; POPC, 1-palmitoyl-2-oleoyl-*sn-glycero*-3-phosphocholine; POPG, 1-palmitoyl-2-oleoyl-*sn-glycero*-3-phospho-(1′-*rac*-glycerol)

1 Introduction

The continuous misuse of antibiotics in the medical and agricultural sectors together with a substantial lack in the discovery of new active molecules has led to a worldwide incidence of multi-drug resistant bacteria. Various international organizations such as the World Health Organization (WHO) and United Nations, as well as the USA government and several European countries, have identified the uncontrolled spread of these resistant microorganisms as one of the most dangerous threats of this century, carrying serious consequences at different social levels, not only in public health but even within macroeconomic sectors [1-5].

Among the alternative solutions to fight bacterial infections, the use of antimicrobial peptides (AMPs) has been considered a very promising strategy given their broad spectrum of activity and rapid bactericidal action [6,7]. AMPs are evolutionarily conserved host-defense molecules found in most complex living organisms, and they selectively target the bacterial membrane through a variety of non-specific interactions. The exploitation of non-specific interactions hinders bacteria from developing definite resistance mechanisms to peptide binding and action [8,9]. Research on AMPs activity during the last three decades have suggested that their interaction with the cytoplasmic membrane could be the first step of the bactericidal mechanism and that inhibition of enzymatic activity, induction of protein degradation, inhibition of protein, nucleic acid or cell wall synthesis, and interference in the transport and energy metabolism could subsequently be involved [8,10,11]. Regarding the first step of their mechanism of action, several scenarios involving or not the formation of pores have been proposed. Among them there are the formation of barrel-stave pores or toroidal pores, a carpet mechanism, sinking raft, lipid clustering and interfacial activity models [11-14]. AMPs have also been found to be active against fungi, viruses, and even cancer cells [15]. Studies aimed at developing AMP-based pharmaceuticals used either engineered synthetic peptides or modified native peptides to improve their antimicrobial properties and stability, and reduce toxicity to host cells. For this to be achieved, a full understanding of the molecular aspects of the AMP-membrane interaction is required. Even if significant advances have been recently done to shed light on the various mechanisms of action of AMPs, some molecular details still remain unknown.

Research about the effects of AMP activity on both biological membranes and lipid bilayer model systems have been performed by means of various experimental techniques [16]. These studies have revealed that the bound-peptide concentration plays a crucial role. The model systems are strongly sensitive to small changes in the peptide-to-lipid (P/L) ratio, requiring low P/L values to observe the peptides' effects, whereas much higher peptide concentrations are needed to obtain significant effects on bacteria [14]. Liposomes are among the mostly exploited model systems to study the interaction of AMPs with lipid bilayers. Liposomes can be classified according to their size and, different sizes allow different techniques to be exploited for their investigation. Whereas Large Unilamellar Vesicles (LUVs, diameter up to about 120 nm) can be used for the analysis of fluorescence signals due to vesicle permeabilization processes at well-established P/L ratios [17], Giant Unilamelar Vesicles (GUVs, diameter from 1 µm up to about 100 µm) can be studied also by optical microscopy techniques including fluorescence techniques [18]. Moreover, GUVs could also be used to investigate the effect of AMPs on the lipid bilayer area changes or on their mechanical properties by using the Micropipette Aspiration Technique (MAT) [19-25] or flickering spectroscopy [26]. At the same time, exploiting GUVs it is possible to establish the effects of mechanical properties modulation on peptide activity [27].

Notwithstanding the variety of biophysical experimental analysis, at present the details about the molecular mechanisms of the AMP/membrane interaction at nanometer scale resolution can be grasped mainly by molecular dynamics (MD) simulations [28-30]. Due to the restrictions in the time covered by simulations and number of included molecules, MD investigations typically target AMPs which are strongly active on lipids which have been well characterized in terms of simulation. This is the case of Magainin H2 (Mag H2), an analog of magainin 2 (*wt* Mag 2) which is one of the best characterized short cationic AMPs. *wt* Mag 2, a 23 amino acids long peptide secreted on the skin of the African clawed frog *Xenopus laevis*, permeabilizes bacterial membranes via toroidal pores without exhibiting significant toxicity against mammalian cells [31-34]. The Mag H2 analog differs on five amino acids that confer it a higher hydrophobicity compared to *wt* Mag 2, consequently enhancing the permeabilizing activity on zwitterionic membranes due to a higher binding affinity, while leaving nearly unchanged its antimicrobial activity [35]. Particularly, Mag H2 shows an ED_{50} for hemolysis of 16 µM, whereas *wt* Mag 2, has practically no activity on red blood cells, and, concerning the bactericidal activity against *Escherichia coli*, Mag H2 has just a four-fold lower MIC with respect to *wt* Mag 2 (2 µM *vs* 8 µM) [35]. This loss of membrane selectivity (zwitterionic host cell *vs* anionic bacterial membranes) might be undesirable from a medical point of view. In fact, due to its activity on zwitterionic lipids, Mag H2 cannot be considered a peptide with therapeutic applications. Nevertheless, in order to infer the molecular details of the peptide/membrane interaction it is important to investigate what happens when the properties of the peptides are changed in order to establish a correlation between the peptide chemical and physical properties and its mechanism of action. On the other hand, zwitterionic lipids such as phosphatidylcholines (PC) are well characterized in MD simulations, and AMPs strongly active on PC membranes like Mag H2 are preferred in this type of studies. In fact, most of the few studies about Mag H2 activity in the literature are of simulation character [30,35-38] whereas the performed experimental studies involved just the analysis of the permeabilization of LUVs [35].

Aimed at filling the gap between simulation and experimental studies about the interaction of Mag H2 with model membranes and at understanding if the different hydrophobicity could induce also a different mechanism of action apart from selectivity with respect to *wt* Mag 2, here we studied the action of Mag H2 on GUVs by using phase contrast optical microscopy, fluorescence microscopy, flickering spectroscopy and MAT. The results have been compared with the results on *wt* Mag 2 taken from the literature. Our results reveal that Mag H2 strongly interacts with lipid bilayers inducing a rapid permeabilization. The permeabilization process is anticipated by a large increase of lipid bilayer area and a strong decrease of the bilayer bending constant. The mechanism of action seems however similar to that of *wt* Mag 2, implying the probable formation of toroidal pores that decrease their diameter as the permeabilization process proceeds. Mag H2 has a strong permeabilization activity on bilayers composed of zwitterionic lipids and is less effective on GUVs including PG or cardiolipin (CL) lipids suggesting that the monolayer curvature

could prevail over the peptide-membrane electrostatic interaction partly inhibiting the formation of pores and the permeabilization process.

2 Material and methods

2.1 Lipids, fluorescent markers and peptides

DOPC (1,2-dioleoyl-*sn-glycero*-3-phosphocholine), POPC (1-palmitoyl-2-oleoyl-*sn-glycero*-3-phosphocholine), POPG (1-palmitoyl-2-oleoyl-*sn-glycero*-3-phospho-(1'-*rac*-glycerol), Cardiolipin (CL) (Heart, Bovine), and cholesterol (chol) were bought from Avanti Polar Lipids (Alabaster, USA). 1,2-dihexadecanoyl-*sn-glycero*-3-phosphoethanolamine-Texas Red (DHPE-Texas Red) was bought from Life Technologies (Thermofisher. Carlsbad, CA, USA). Carboxyfluorescein (CF) was bought from Sigma-Aldrich Corporation (Saint Louis, MO, USA). Specific lipid mixtures were prepared by mixing chloroform lipid solutions in the desired amount (the proportions used in this work are to be intended as molar). The peptide Mag H2 (Ile – Ile – Lys – Lys – Phe – Leu – His – Ser – Ile – Trp – Lys – Phe – Gly – Lys – Ala – Phe – Val – Gly – Glu – Ile – Met – Asn – Ile) was purchased in powder from United BioSystems Inc, with a 95.6% purity, and used without further purification (see Par S1 and Fig. S1 for the aminoacid sequence and hydropathy of Mag H2 compared to the natural Magainin 2). It was dissolved in Millipore water at a high peptide concentration (4 mg/mL) and stored at −20 °C until required for use.

2.2 Preparation of GUVs

GUVs were prepared according to the usual electroformation method [39] with minor modifications. Briefly, lipid mixtures were suspended in chloroform, and small drops (2–3 µL from a 2 mg/ml lipid solution) were deposited on two opposing platinum (Pt) wires positioned inside a Teflon chamber. The chloroform was initially removed via a Nitrogen flux and then the chamber was positioned inside a vacuum system (10^{-2} mBar) for 0.5–1 h. Thereafter, the Pt wires were connected to an electric function generator providing a sinusoidal voltage potential difference. The Teflon chamber was then filled with a 100 mM sucrose solution, and sealed. The electroformation protocol was as follows: (i) 10 Hz, 4.0 $V_{p\text{-}p}$ for 105 min; (ii) 5 Hz, 2 $V_{p\text{-}p}$ for 45 min; (iii) a 5 Hz square-wave for 5 min in order to promote the final detachment of the vesicles from the wires. All the procedure was performed at a temperature of 40 °C. GUVs were then extracted from the Teflon chamber and resuspended in a 105 mM glucose solution. The presence of the osmotic difference across the bilayer (the external glucose concentration is 5 mM higher than the sucrose concentration) makes the vesicles a little bit flaccid increasing their bending fluctuations, and approaching the behavior of biological membrane which are typically not tensed. When GUVs were prepared for fluorescence microscopy investigation, a 0.5–1% molar amount of DHPE-Texas Red was included in the lipid mixtures in order to mark the bilayer. When studying Mag H2-induced membrane permeabilization via fluorescence microscopy, CF was added to the imaging or formation medium. In the first case, we measured the influx of CF, and we injected the GUVs in a chamber already containing 10 µM CF in 105 mM glucose + the desired Mag H2 concentration. In the second case, we formed the vesicles in the presence of 100 mM sucrose + 10 µM CF. The vesicles were then washed by at least 5 cycles of centrifugation and exchange of the supernatant with 105 mM glucose before injecting them in a chamber already containing the desired concentration of Mag H2. The chambers we used to study the permeabilization of the GUVs were made with glass slides and Teflon and the bottom glass surface was pretreated with BSA (10 mg/mL) to avoid adhesion between glass and lipid bilayers. The BSA solution was then removed and the chamber abundantly rinsed with the working solution. We did not observe any effect ascribable to residual BSA in the chamber.

2.3 Micropipette aspiration

Micropipettes were made by pulling glass capillaries (World Precision Instruments, Sarasota, FL, USA) of 1.2 mm initial-internal diameter, reaching a final cylindrical shape and an internal diameter of ~10 µm. To pull the micropipettes, we initially used a HEKA temperature controlled pipette puller PIP5 followed by the use of a home-developed pipette puller to obtain the final cylindrical shape. A home-made microforge was used to cut the micropipette perpendicularly to its axis; the capillaries were then tip-polished to smooth their break-point in order to ensure good membrane/micropipette contact. The micropipettes were pretreated with BSA (10 mg/mL) to avoid adhesion between glass and lipid bilayers by neutralizing the charge on the bare glass surface, and then the pipettes were abundantly rinsed with the working solution. The micropipettes were then filled with a 105 mM glucose solution, assuring the absence of internal air bubbles. Finally, the micropipette is connected to the aspiration system, and immersed in a home-made Teflon/glass chamber where the vesicles were deposited.

To apply lateral tensions to the vesicles, the micropipette was connected to a pneumatic pressure transducer (Lorenz MPCU-3) to exert pressure differences between the internal side of the pipette and the external solution at the same height, with a sensitivity of 0.1 cm H_2O. The pressure difference was applied by controlling the air pressure on top of a cylindrical tube containing the same external solution and initially kept at the height providing a negligible pressure difference. The negligible initial pressure was evidenced by the absence of movement of small particles in front of the pipette aperture. Controlling the height difference of the solution levels in two tubes, we are able to aspirate the vesicle into the micropipette, and the progressive membrane deformation (projection) into the micropipette can be measured as a function of time at constant pressure difference. To study the kinetics of the interaction of the molecules with a lipid bilayer, a fast perfusion system would be required (the measurement time should start with an already established constant concentration of the peptides). To circumvent this problem, we assembled a cell with two chambers [23,25,40], and we transferred the vesicles to be studied from one chamber without the peptide to another chamber with the already homogeneous peptide concentration. In particular, the chambers are prepared using Teflon in order to have a hydrophobic surface and to avoid the contact between the liquids of the two compartments (see Fig. S2). To better insulate the two compartments we also used two small pieces of a Teflon foil (25 µm thick) in contact with the glass in the channel. One compartment is filled with the vesicle solution in glucose. Using a micromanipulator, a pipette with an external diameter of about 0.5/1 mm and filled with the glucose

solution is inserted through the hole from the compartment opposite to the vesicle in order to reach the vesicle solution. The other compartment is then filled with the solution already containing the Mag H2 concentration we want to investigate. A vesicle from the first compartment is aspirated by the micropipette and the vesicle with the micropipette are then inserted inside the bigger pipette (see Fig. S2). The chamber is then moved by using the microscope stage in order to take the aspirated vesicle to the chamber containing the peptide solution. The bigger pipette is then removed and the interaction kinetics starts. Time t = 0 in our analysis corresponds to the removal of the bigger pipette and the exposure of the vesicle to the Mag H2 solution. All the formulas used to analyze the experiments performed by MAT are reported in the Supplementary Material section (see Par S2).

2.4 Flickering spectroscopy

GUVs have been observed using 40X phase contrast objective (NA 0.60), mounted on an Olympus IX 70 microscopy. An additional lens incorporated in the microscope was used to increase the total magnification, up to 60X. A CCD high-resolution video camera (QIcam FAST Cooled Mono 12-bits) was used to store GUVs movies of 1500 phase images with a frame rate of 25 images/s, and an integration time of 15 ms. The samples have been prepared using an O-ring chamber sealed with two cover glasses. During sample preparation, GUVs were suspended in 112 mM glucose solution in order to make fluctuations easily visible by optical microscopy at our resolution level. The images of fluctuating vesicles represent the evolution in time of the GUVs contour at the equatorial plane. Using a home-made software developed in Python, the vesicle contour for each image of the sequence is detected with a sub-pixel resolution [41]. The 2D contour coordinates are used to obtain the radial fluctuations: $r\left(\frac{\pi}{2},\varphi,t\right)=r(\varphi,t)$ in polar coordinates at the equatorial plane at a given time t, corresponding to the analyzed image.

Starting from radial fluctuations, the angular autocorrelation function is evaluated by:

$$\xi(\gamma,t)=\frac{1}{2\pi R^2}\int_0^{2\pi}[r(\varphi+\gamma,t)-r(t)]\cdot[r(\varphi,t)-r(t)]\,d\varphi \quad \textbf{(1)}$$

where $r(t)=\frac{1}{2\pi}\int_0^{2\pi}r(\varphi,t)\,d\varphi$ is the averaged radius of the vesicle, and $R=\sum_{i=0}^{Nf}\frac{r(t_i)}{N_f}$ is the mean radius obtained from the entire sequence containing N_f frames. The autocorrelation functions are then decomposed using a Legendre Polynomials basis, $\xi(\gamma,t)=\langle B_0\rangle P_0(\cos\gamma)+\sum_{n=2}^{N_{\max}}\langle B_n\rangle\cdot P_n(\cos\gamma)$, obtaining the corresponding B_n coefficients for each frame. Finally, the mean value $\langle B_n\rangle=\sum_{i=0}^{Nf}\frac{B_n(t_i)}{Nf}$ is evaluated. Using a Levenberg-Marquardt procedure, the experimental $\langle B_n\rangle$ values are fitted following the theoretical expression:

$$B_n(\kappa,\bar{\sigma})=\frac{2n+1}{4\pi}\cdot\frac{k_bT}{\kappa(n+2)(n-1)[\bar{\sigma}+n(n+1)]} \quad \textbf{(2)}$$

where k_b is the Boltzmann constant, κ and $\bar{\sigma}$ are the bending constant and the reduced surface tension, respectively, and $n>1$. For the fitting procedure, coefficients between the 3° and 154° mode number were used. Since the coefficients are defined as greater than 0, following Eq. (2), all negative contributions have been neglected.

2.5 Fluorescence microscopy

Epifluorescent images were acquired using an Olympus IX 70 microscope equipped with a 20X or 40X objective (NA 0.4 and 0.75, respectively). All procedures were performed at minimal light exposition (using neutral filters) to avoid fluorophores' photobleaching. A CCD high-resolution video camera (QIcam FAST Cooled Mono 12-bits) or a CMOS camera (Hamamatsu ORCA-flash 4.0LT - C11440) connected to a computer were used for image and video capture. Analysis of images and videos was made using ImageJ [42]. For confocal imaging, we used a Leica SP2 microscope with AOBS (Acoustic Optical Beam Splitter), and 40X and 63X-oil immersion objectives. The excitation wavelengths for CF and Texas-Red were 488 nm and 594 nm, respectively; the emission wavelengths were 517 nm and 615 nm, respectively as well. Analysis of the evolution of the fluorescence intensity inside GUVs was performed with ImageJ+Time Series V3 plugins. Briefly, the images corresponding to the time sequence of each vesicle, were selected, properly aligned, and joined in a single sequence. Images corresponding to the fluorescence reference value (outside the vesicle) were inserted in the sequence, as well.

3 Results and discussion

3.1 Strategies for the study of the permeabilization of GUVs by peptides

Typically, three different strategies can be exploited to verify the permeabilization activity of AMPs on GUVs: (i) the GUVs being inside a chamber, the AMPs are delivered by using a micropipette positioned near to a single vesicle (single GUV method); (ii) the vesicles are injected in a glucose solution already containing a homogeneous peptide concentration (GUV dispersion method); (iii) the vesicles are injected in a chamber and, after they have been settled down, the peptides are injected into the medium. Among them, just strategy (ii) allows the measurement of the peptide-vesicle interaction at a well-defined AMP concentration. Obviously, the adsorption of the peptides on the vesicles implies a decrease of the peptide concentration in solution but, in most cases, it can be considered anyway as an equilibrium situation given the usually high amount of peptides in solution in experiments involving GUVs. This

strategy presents the impossibility of having data at a very short time after exposing the vesicle to the peptides because enough time has to elapse (about 40–50 s) before the vesicles settle at the bottom of the imaging chamber in order to have a time lapse visualization of their state. In strategy (iii) the exact peptide concentration near to the GUVs is not known, or it changes during the measurements. When GUVs are exposed to a peptide flux (strategy (i)), vesicles not adhering to the surface are easily moved. Vesicles not moving are probably physically adhered to the substrate, and this condition could alter the tension in the bilayer. If the possibility of blocking the vesicles on the support by a specific chemistry such as biotin/avidin is exploited [43], it is possible to flux a solution with a well-defined peptide concentration and this method, repeated on several vesicles, could provide valuable results even if the uncertainty on the concentration and effects related to mass diffusion in solution should be considered. Different methods of vesicles exposure to peptides could give different results. In the experiments performed in this study, we mainly worked with strategy (ii), i.e. the vesicle dispersion method. With this method we never measured the permeabilization kinetics. What we were able to measure is the percentage of intact and permeabilized vesicles after a quite long interval from the vesicle injection (about 30 min) or the kinetics of influx or efflux between the vesicle lumen and the external solution from the moment when these events start. In these cases, we considered time t = 0 as the time at which the permeabilization starts without reporting the real time after the initial exposure of the vesicles to the Mag H2 solution. The overall time at which the influx or efflux start is stochastic. More results obtained with the other strategies are reported in the Supplementary Material Section.

3.2 Role of lipid composition on the Mag H2 effect

In order to identify which types of lipids could promote or disfavor the permeabilization effect of Mag H2, GUVs with different lipid compositions have been studied. We initially measured the percentage of permeabilized vesicles for different lipids and for different peptide concentrations after 30 min incubation time with Mag H2 [44,45]. For this analysis we exploited phase microscopy imaging. The permeabilization efficiency is detected by the contrast change due to an equilibration process between sucrose inside the GUV and glucose outside the GUVs once pores have been formed. To be sure that the leakage process by itself could not affect the time analysis, we followed the leakage process of several vesicles by time lapse phase contrast imaging with a time resolution of just a few seconds. Fig. 1 reports a representative example for a DOPC/chol (88%/12%) vesicle.

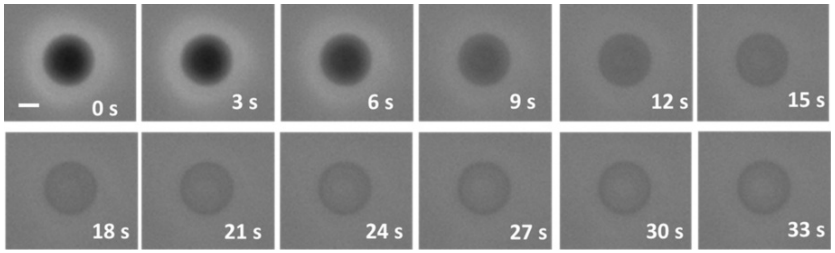

Fig. 1 Sequence of phase contrast optical microscopy images of a DOPC/chol (12% cholesterol molar content) GUV exposed to a 2 μM Mag H2 concentration. Once it starts, in about 30 s all the permeabilization process is complete. The contrast loss is related to equilibration of the internal (sucrose) and external (glucose) solutions of the GUV. The time reported on each image starts from the starting of the vesicle leakage (bar = 10 μm).

Once it starts, the leakage process reaches an equilibrium situation in about 30 s. In some cases, the leakage process was not complete but it stopped producing a partially permeabilized situation. This scenario was more evident at low peptide concentrations for all the lipid compositions we studied. Anyway, in the case of partial permeabilization, after a fast first step (see below) a second very slow leakage process follows. The fact that the leakage process is much faster than the observation time of 30 min assures us that it is the rate of pore formation what is relevant, and not the time required for the equilibration of the internal and external solutions of the GUVs. Table 1 reports the percentage of still intact vesicle at the end of the 30 min incubation time for different lipid composition of the GUVs.

Table 1 Permeabilization effect of Mag H2 at different concentrations for GUVs with different lipid compositions, estimated as the fraction of not-permeabilized vesicles after ≈30 min. All the measurements have been performed at a constant controlled temperature of 27 °C, and more than 100 vesicles have been considered for each experiment. Each experiment was repeated 3 times giving consistent results. The reported error is the standard deviation of the repetition of the experiments (n = 3). ND = Not Determined.

Compositions	*Percent of intact GUVs after 30* min	
	1 μM Mag H2	2 μM Mag H2
DOPC	ND	26 ± 9
POPC	47 ± 7	0.3 ± 0.1
POPC/POPG 3:1	73 ± 10	30 ± 8

DOPC/chol 88:12	ND	32 ± 10
DOPC/chol 76:24	ND	79 ± 8
DOPC/chol 60:40	ND	84 ± 12

As a first analysis, we compared the permeabilization activity of Mag H2 on DOPC and POPC vesicles in order to understand the role of chain unsaturation on the activity of Mag H2. Due to its higher hydrophobicity, Mag H2 is much more effective on PC lipids than Mag 2 and very low concentrations of Mag H2 are enough to induce permeabilization of the vesicles (1–2 μM) whereas concentrations starting from 15 μM are required for Mag 2 [46]. The fraction of not-permeabilized vesicles shown in Table 1 reveals that DOPC bilayers are more resistant to Mag H2 permeabilization than POPC bilayers. This is quite interesting because DOPC, having two unsaturated chains, is expected to be more disordered than POPC at the same temperature (the analysis have been performed at a controlled temperature of 27 °C) and more prone to be destabilized by the peptide. A possible explanation for this behavior is related to the spontaneous curvature of the monolayers. In fact, given the increased volume of the acyl chain region of DOPC monolayers, it is expected that they will have a higher tendency to adopt negative curvature with respect to POPC monolayers. Experimental data on the spontaneous curvature for DOPC and POPC report a higher negative curvature for DOPC ($-0.091\,nm^{-1}$) with respect to POPC ($-0.022\,nm^{-1}$) [47]. Given that simulations of the activity of Mag H2 show the formation of toroidal pores [30], lipids with a higher negative curvature will protect the bilayer from the formation of Mag H2 pores [48]. The same protective behavior was observed in vesicles containing CL (see Par S5), a lipid with the tendency to form monolayers with high negative curvature, and to easily adopt the inverted hexagonal phase structure (H_{II}).

We then compared the permeabilization activity of Mag H2 on vesicles including negatively charged lipids -such as POPG- in order to understand their role on the activity of Mag H2. We found that a POPC/POPG (3:1) lipid bilayer is more protective than a pure POPC bilayer (Table 1). It is important to point out that the measurements in this case were performed in water plus 105 mM glucose without any buffering agent, obtaining a solution with pH between 5 and 5.5 that assures a negative charge to the PG headgroup (the pK_a of phosphatidylglycerol is ~3). In the case of Mag 2, it has been found in previous works that the presence of PG favors the permeabilization of the vesicles [46]. The presence of negatively charged lipids typically increases the effect of cationic AMPs due to the electrostatically increased adsorption of peptides on the lipid bilayer. This is exactly what happens in the case of Mag 2, while in the case of Mag H2 the presence of PG acts as a protection against permeabilization. It is also to be stressed that in water solution (even if residual Na^+ ions are present in the solution according to how lipids are provided by Avanti Polar Lipids) the electrostatic effect is even more intense with respect to buffer solutions in which the charges are shielded, and the tendency to adopt inverted phases is reduced. In other cases, it has been recently found that the electrostatic force is relevant in the AMP/lipids interaction but it is not the only relevant parameter and, in specific cases, the geometry of the bilayer, the number of defects and the lipid-to-lipid average distance could overwhelm the electrostatic interaction [49]. The protective effect of PG groups is present for both 1 and 2 μM Mag H2 concentrations that we analyzed (Table 1). A similar result has been obtained in the case of LUVs [35] and it has been interpreted as a result of the intrinsic more negative curvature of PG with respect to PC [50]. Even in this case it is important to highlight that our experiments could be different with respect to experiments performed in buffer solution; in particular, the higher negative curvature value for PG is reported for buffer solutions; therefore, in our case, the presence of the positively charged peptides could play a role similar to poly-electrolytes in solution. Our results suggest that, for Mag H2-induced permeabilization, the intrinsic monolayer curvature could be more relevant than the electrostatic interaction between the peptide and the bilayer. Another case in which a protective effect of POPG lipids has been obtained is related to a modification of the maculin peptide by the insertion of a proline amino acid [51].

We also evaluated the role of cholesterol on the permeabilization activity of Mag H2. Cholesterol has typically a protective effect against AMPs, and this aspect is one of the mechanisms conferring specificity to the activity of AMPs towards bacteria with respect to host-cell membranes [52]. We demonstrated that cholesterol has a protective effect also in the case of Mag H2. Whereas in the case of DOPC/chol (with cholesterol molar content equal to 12%) the fraction of permeabilized vesicles is comparable to the case of pure DOPC, at a cholesterol molar fraction of 24%, the protective effect is greatly enhanced, and it seems to reach a saturation effect for larger concentrations considering that 40% cholesterol concentration provides similar results (Table 1). A similar non-linear behavior as a function of cholesterol concentration has already been obtained for MSI-78 [53], a 22 amino acids long AMP commercially known as pexiganan. The non-linear behavior has been interpreted as the result of a phase change of the DOPC/chol binary mixture for cholesterol concentrations higher than ~20%. In fact, for cholesterol concentrations above 20%, regions of L_o phase should form, and the activity of the peptides on these domains should be strongly inhibited. We speculated that the protective effect of cholesterol is mainly related to its effect on the phase state of the bilayer and on their mechanical properties; in fact, the presence of cholesterol in lipid bilayers confers a much higher value to the their stretching and bending constants [54]. On the other hand, in many cases, the formation of black dots or spots on the surface of vesicles was observed by phase contrast microscopy after the exposure to the peptide, in particular in the case of vesicles containing CL (see Fig. S7 and Fig. S12a). By including 1% DHPE-Texas Red in the bilayer of the vesicles, we were able to confirm that the black dots are due to lipid accumulation (see Fig. S12b); for example, in case of high Mag H2 concentrations, we observed formation of large spots on the surface of the vesicles before they collapse (see Fig. S6). Furthermore, the presence of these spots does not imply the permeabilization of the involved vesicle. We do not know which could be the organization of the lipids within these regions, and we just refer to these structures as accumulation of lipids, as suggested also by other studies [55,56].

3.3 Quantitative analysis of the influx kinetics

For a quantitative analysis of the kinetics of the influx process we exploited a fluorescent dye and confocal microscopy using strategy (ii). Fig. 2 shows GUVs composed of POPC +1% DHPE-Texas Red dispersed in a solution containing 105 mM glucose + 10 μM CF. Even in this case the exact P/L ratio is difficult to establish due to the impossibility of knowing the lipid concentration in the sample. Fig. 2a shows the vesicles in the absence of Mag H2. At the beginning of the experiment, the internal region of the GUVs showed the complete absence of CF. On the time scale of several minutes no permeabilization event was observed in the absence of the peptides. Vesicles exposed to Mag H2 showed different behaviors depending on the peptide concentration. In all the reported experiments, time t = 0 corresponds to the starting of the influx of efflux process, independently from the overall time of exposure of the GUVs to the peptide. Fig. 2b shows the effect of a 1 μM Mag H2 concentration on POPC GUVs. In this case most of the vesicles become partially permeabilized: after an initial rapid influx of CF molecules, the flux slows down, and it proceeds at a very low rate probably due to a size reduction of the pore diameter (see also Fig. S3 for a photobleaching experiment, and Fig. S4 for an example of influx kinetics after the initial fast step). The decrease of the pore size after the initial influx (or efflux) of a dye has been already reported both for Mag 2 [57] and for Mag H2 [35]. Fig. 2c shows a completely permeabilized vesicle which was exposed to a 2 μM peptide concentration. The same behavior was observed for both CF influx and efflux. The behavior of the influx process for some of the analyzed GUVs is shown in Fig. 3. To analyze quantitatively the data, we used a simple exponential decay function similar to the one reported in [58]:

$$I(t) = (1 - A) + Ae^{-kt} \quad \textbf{(3)}$$

where $I(t)$ represents the difference of the fluorescence intensity between the external region and the region inside the vesicle, normalizing to 1 the difference at time t = 0 when no permeabilization has occurred, (1-A) is the permeabilization fraction (where A is the percentage of fluorescence increase inside the vesicle. A = 1 would correspond to a total permeabilization of the vesicle), and k is the inverse of the time constant (in s^{-1}). Before fitting the data with the exponential function, we aligned the fluorescence intensity trends so that $t = 0$ s corresponds to the stochastic beginning of the CF influx process. The rate constant k is about (0.048 ± 0.016) s^{-1} (mean ± s.d. for n = 9) in the case of partial permeabilization (Fig. 3a–c), and (0.041 ± 0.012) s^{-1} (mean ± s.d. for n = 9) for total permeabilization (Fig. 3d–f). The permeabilization of the vesicles loaded with CF (efflux kinetics) occurs on similar time-scales (see Fig. S5). We also performed an analysis of the initial volume flux J_V across the bilayer in the cases of both transient and complete permeabilization exploiting the method presented in [44,45] (see Par S4). The results are reported in Fig. 4 showing that by doubling the Mag H2 concentration from 1 μM to 2 μM we have an initial dye influx changing from (0.04 ± 0.02) μm/s to (0.29 ± 0.08) μm/s (mean ± s.d, n = 9) . This result can be interpreted as an increased number of pores initially formed at higher Mag H2 concentration leading to a complete influx of the dye during the period in which the pores remain completely open. In the case of partial permeabilization, the number of pores could be not enough to obtain a complete equilibration of CF concentration during their open time.

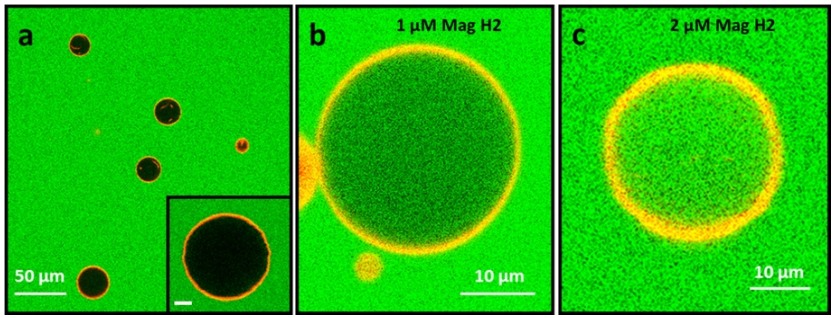

Fig. 2 Confocal fluorescence microscopy images of POPC+1% DHPE-Texas Red GUVs dispersed in a solution containing 105 mM glucose + 10 μM CF. (a) GUVs not exposed to Mag H2; scale bar in the inset = 5 μm; (b) example of a POPC vesicle partially permeabilized after exposing the GUVs to a 1 μM Mag H2 concentration; (c) example of a vesicle completely permeabilized after being exposed to a 2 μM Mag H2 concentration. (For interpretation of the references to colour in this figure legend, the reader is referred to the web version of this article.)

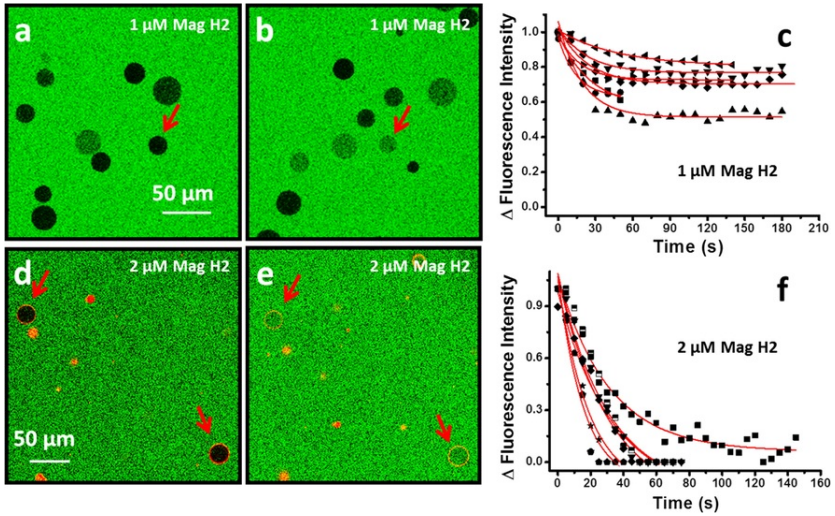

Fig. 3 Analysis of the influx kinetics of a POPC GUV by confocal microscopy. (a) and (b) POPC GUVs dispersed in a solution containing 105 mM glucose + 10 µM CF, exposed to a 1 µM Mag H2 concentration. A GUV initially not-permeabilized (indicated by a red arrow in panel (a), appears partially permeabilized 200 s later (indicated by a red arrow in panel b – the vesicles slowly moved in the chamber and we had to follow their positions); (c) normalized fluorescence signal difference between the regions outside and inside the vesicles. The black dots correspond to representative traces of the kinetics of the fluorescence marker influx whereas the red continuous lines represent the best fit by Eq. (1). The influx process occurs by an initial fast step corresponding to the opening of the pores, followed by a very slow influx process which is not noticeable on this time scale; (d) and (e) POPC GUVs dispersed in a solution containing 105 mM glucose + 10 µM CF, exposed to a 2 µM Mag H2 concentration. Two GUVs initially not-permeabilized (indicated by the red arrows in panel (d)) appear completely permeabilized in panel (e); (f) normalized fluorescence signal difference between the regions outside and inside the vesicles. The black dots correspond to representative traces of the kinetics of the fluorescence marker influx whereas the red continuous lines represent the best fit by a simple exponential decay function. All the curves have been aligned in such a way that t = 0 s corresponds to the beginning of the influx process for all the vesicles. (For interpretation of the references to colour in this figure legend, the reader is referred to the web version of this article.)

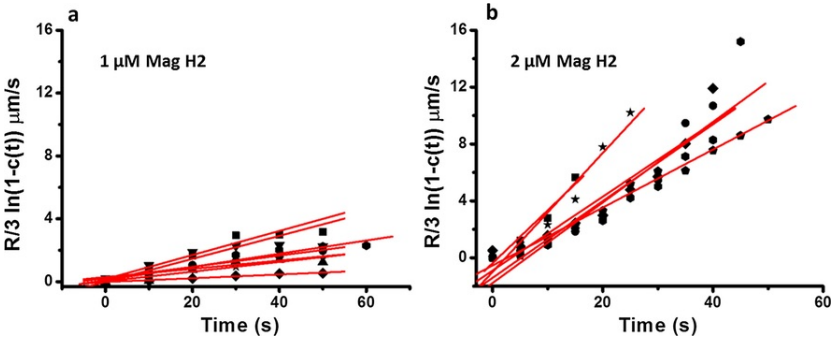

Fig. 4 (a) Log-linear plots of time-dependent initial dye influx (−R/3ln(1 − c)) versus time for partial permeabilization of POPC GUVs exposed to 1 µM Mag H2 concentration. The average flux value is (0.04 ± 0.02) µm/s (average ± sd); (b) The same plots as in (a) in the case of POPC GUVs exposed to 2 µM Mag H2 concentration in the case of total permeabilization. The average flux value is (0.29 ± 0.08) µm/s (average ± sd).

If Mag H2 concentration is further increased to greater than 5 µM, we observed a very fast complete influx kinetics with the GUVs rapidly losing their stability resulting in the formation of spots where lipids accumulate as evidenced by the localized increase of the lipid fluorescence signal (see Fig. S6). The partial permeabilization phenomenon can be interpreted on the basis of the fact that once the pores are formed, they can close or reduce their size even if we do not know the mechanistic details of this phenomenon. In this case, the level of permeabilization depends on the rate constant of the fluorophore flux: if the flux rate is high (large pores or high number of pores for example), it is possible to obtain a complete permeabilization before pore closure or size reduction, whereas if the flux is slow (narrow pores for example), the vesicles will show just a transient permeabilization followed by a second phase characterized by a very low permeabilization rate (~0.0019 s^{-1}, see Fig S4). This behavior could also be interpreted in the context of the translocation of the peptides from one leaflet to the other. From our results, in the case of

Mag H2 the behavior is mainly related to its concentration and to the initial value of the influx of the fluorescent dye.

3.4 Investigation by micropipette aspiration of GUVs exposed to Mag H2

The MAT technique is typically exploited to study the mechanical properties of lipid bilayers in the form of GUVs or to investigate the bilayer area expansion or volume variation providing information about the interaction kinetics of the lipid bilayer with exogenous molecules [20-25]. Usually, to study the interaction of the lipid bilayer with exogenous molecules, a single GUV is grabbed by a micropipette which is covered by a bigger pipette, and moved to a different compartment already prepared with a solution of homogeneous concentration of the molecule of interest. The removal of the bigger pipette marks the beginning of the interaction kinetics [25,59]. The expansion or retraction of the vesicle area is detected by the movement of the vesicle projection inside the micropipette (increase or decrease, respectively) which works as an amplifier of the effect of the peptides on the bilayer area (see the Supplementary Information Par S2 for details of the analysis). The data we will show are mainly representative of the qualitative behavior of the lipid bilayer exposed to the peptides given that a rigorous quantitative analysis in terms of peptide concentration could strongly depend on the initial conditions, such as vesicle size and applied lateral tension.

MAT experiments on DOPC GUVs at different Mag H2 concentrations were performed. Fig. 5a–c shows the results of the exposure of a DOPC GUV to a 5.37×10^{-13} M Mag H2 concentration [40], corresponding to P/L ≈ 1/30 (to obtain this estimate we considered that there is only one GUV in the chamber, the vesicle is composed by approximately 5.8×10^{9} lipids according to its size and the area-*per*-lipid and we evaluated the total number of peptides in the chamber on the basis of the peptide concentration and the volume of the chamber ~0.6 mL). From all the performed experiments (n = 7) at this peptide concentration, in ~70% of the cases the projection increased like in the case shown in Fig. 5a-c, whereas in the remaining 30% the vesicle projection remained stationary. Fig. 5g shows the relative area increase associated with the overall projection increase as a function of time for two representative experiments. When the Mag H2 concentration is increased to 10^{-9} M, we observed the opposite effect, i.e. the vesicle projection retracted such as in the sequence shown in Fig. 5d-f (n = 5). The retraction rate depended on the Mag H2 concentration, increasing with peptide concentration, as shown in Fig. 5h. In the case of the vesicle projection retraction we did not analyze its behavior in terms of relative area variation because it cannot be excluded that the lipid bilayer is adopting structures in which lipids accumulate in some points, having an effect on the quantitative analysis. In fact, in some cases we observed the formation of dots on the lipid bilayer during the projection retraction. Qualitatively, the decrease of the vesicle projection can be interpreted as due to a volume increase of the vesicle. In this case, the volume increase could be related to the formation of pores in the membrane inducing the influx of glucose molecules in the vesicle lumen.

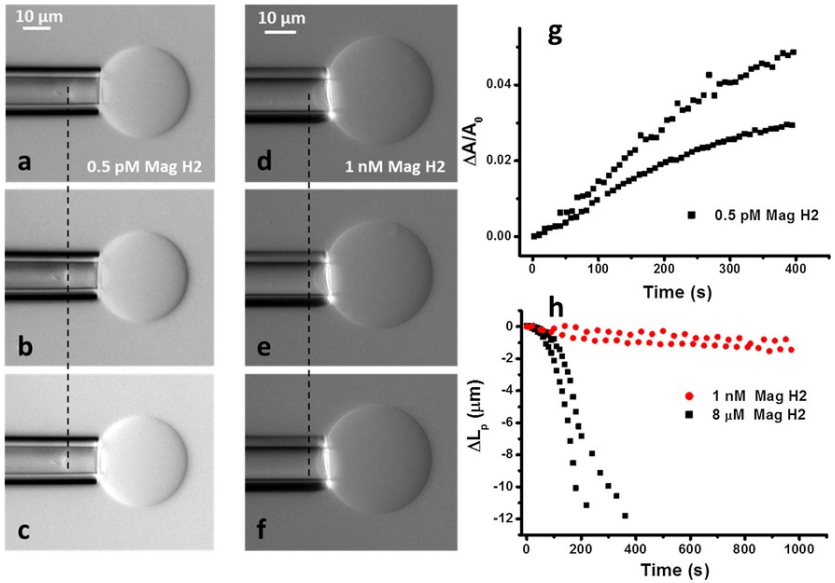

Fig. 5 (a)–(c) Evolution of the vesicle protrusion inside the micropipette for a DOPC vesicle (t = 0 s, 150 s, 350 s, respectively) exposed to a 5×10^{-13} M Mag H2 concentration. The vertical dashed line highlights the position of the vesicle projection inside the micropipette with respect to the first snapshot; (d)–(f) sequence of images acquired on a DOPC vesicle exposed to a Mag H2 concentration of 10^{-9} M. The lipid bilayer protrusion retracts as a consequence of the interaction with the peptides; (g) evolution of the relative area variation as a function of time for two representative cases for 5.13×10^{-13} M Mag H2; (h) representative plots of the protrusion retraction for two Mag H2 concentrations, 10^{-9} M (black squares) and 8 µM (red circles). In the case of the 8 µM concentration, the vesicle disrupted after 200 s. (For interpretation of the references to colour in this figure legend, the reader is referred to the web version of this article.)

Considering the extreme sensitivity of the bilayer to the peptide concentration, and looking for the transition from the expansion to the retraction behavior on the same vesicle, we decided to change the method of vesicle exposure to the peptides. To this aim, we grabbed one POPC vesicle using the MAT system, and then injected in the chamber a peptide amount equivalent to a final concentration of 2 and 4 μM without any stirring procedure. By this way, the concentration of the peptide near the vesicle increases as the diffusion of the molecules proceeds. Before injecting Mag H2, we measured the background effect on the position of the vesicle projection inside the micropipette due to the evaporation of water in the imaging chamber. Fig. 6 shows the trend of the relative area variation as a function of time for different POPC vesicles. For 2 μM Mag H2, we generally observed a slow increase of the area up to a relative variation of 4% followed by a projection retraction and the final collapse of the vesicle. For 4 μM Mag H2, the typical behavior consists of an initial rapid area increase, a decrease of the growth rate which is then followed, after a relative area variation of about 8%, by a rapid retraction of the vesicle projection; the sequence ends with the collapse of the vesicle (see Movie S1 for the complete sequence of one experiment). The average area increase for the two concentrations, 2 and 4 μM, are 3.3 ± 1.0% and 6.3 ± 1.6% (n = 9 in both cases), respectively. The behavior of the vesicle projection can be explained as follows: an initial area increase takes place due to the adsorption of the peptide and the decrease of the lipid bilayer thickness (it is not excluded that a contribution comes also from the decrease of the bending constant – see below – of the lipid bilayer affecting the GUV projection position). It is to be stressed that the second region of slow increase of the area should be considered taking into account also the reported area variation just due to solvent evaporation (thin dashed line in Fig. 6). If this effect is taken into account, we can say that after the initial increase, the lipid bilayer area stays constant until the permeabilization and the increase of the volume starts. This behavior is similar to the one observed for Mag 2 in ref [19]. The increase of the volume always leads to the destruction of the vesicle, probably due to the strong effect of the peptide on the mechanical properties of the bilayer and the lateral tension applied by the micropipette.

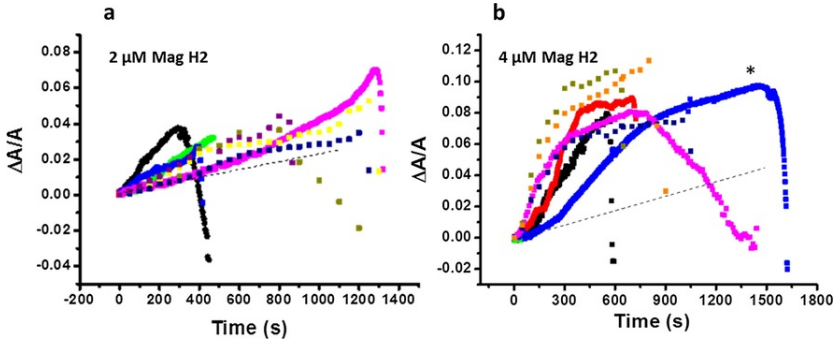

Fig. 6 Evolution of the relative area change as a function of time of POPC GUVs exposed to (a) 2 μM and (b) 4 μM Mag H2 concentrations. The dotted light grey line represents the extrapolation of the drift of the relative area variation due to water evaporation measured for 500 s in (a) and 200 s in (b) on the same vesicle at the beginning of each experiment. (see movie S1 for the experiment indicated by the asterisk).

3.5 Vesicle area variation before permeabilization

We then tried to deepen the understanding of the lipid bilayer changes while it interacts with Mag H2 before the permeabilization process starts. To do this, we decided to continuously follow the shape changes of the vesicles during the exposure to the peptides by measuring the equatorial shape of the vesicles using phase contrast imaging. We then reconstructed the approximate perimeter of the equatorial image of the vesicle using the same profiling technique exploited for flickering spectroscopy (see below) and, at the same time, we measured the changes of the phase contrast inside the vesicles as a marker of the permeabilization process. In this case we can report the ratio between the average contrast inside the vesicle and the average contrast value measured outside the vesicle as a function of time. The initial contrast difference between the two regions is due to the fact that the solution inside the vesicle contains sucrose whereas outside it is mainly glucose. Upon permeabilization, the solutions inside and outside the vesicle equilibrate and the ratio approaches 1. Fig. 7 shows an example for this kind of analysis on a POPC vesicle exposed to 2 μM Mag H2. If a GUV had a spherical shape it could be possible to measure the area from the measurement of the circle obtained at the equatorial region. In the case of a fluctuating vesicle, the measurement of the perimeter at the equatorial region can be exploited only to have an idea of fluctuations but not as a parameter from which to obtain the exact vesicle area. Accordingly, the trend of the perimeter reported in Fig. 7 shows the behavior of the fluctuations as the interaction of the vesicle with Mag H2 proceeds. The images reported in Fig. 7 show the vesicle frames at the different time points reported in the plot (the complete sequence of images is reported in Movie S2). As already pointed out, the first effect of peptides adsorbing onto the lipid bilayer is an increase of the visible lipid bilayer fluctuations. Both, the excess area and the possible thickness decrease could induce this effect as well as a bending constant decrease. The increase of fluctuations however proceeds without any change in the phase contrast between the internal and external regions of the vesicle (the instabilities in the plot of Fig. 7 are due to the overlapping of floating structures in the chamber as it is evident from Movie S2). At point 3 in the plot, fluctuations of the bilayer rapidly decrease without producing any change in the internal contrast of the vesicle. We tentatively associate this phase to the translocation of the peptides from the external to the internal leaflet of the bilayer. Immediately after this rapid phase, the permeabilization starts and the area of the vesicle increases. In the Supplementary Material section we report the analysis of the area variation measured by phase contrast for POPC vesicles exposed to different Mag H2 concentrations (Fig S11) as well as a sequence of images obtained by confocal microscopy showing a similar process (Fig S8). The sequence of the events could be summarized in the following steps: (i) the peptides adsorb onto the external vesicle leaflet increasing its area and generating a strong asymmetry between the two leaflets,

introducing softening of the bilayer and strong visible fluctuations; (ii) the internal leaflet of the bilayer expands due to the interleaflet coupling, probably inducing the formation of highly disordered structures which allow (iii) the translocation of the peptides to the internal leaflet restoring a symmetry between the two leaflets and recovering the spherical shape of the vesicle; (iv) after restoring the spherical shape with a symmetric situation for the two leaflets, pores are formed and the equilibration of the internal and external solutions starts with an increase of the vesicle volume. The behavior that we observed for vesicles exposed to Mag H2 is in part consistent with a model developed for Mag 2 in the literature [57] and is also consistent with experimental results in which fluorescently labeled Mag 2 accumulation on the surface of a GUV has been tracked together with the efflux from the vesicle of a fluorescent species [19]. In particular Karal et al. [19] show the presence of a small lag time between the moment in which the peptide starts to translocate to the inner leaflet of the vesicle and the starting of the fluorescent dye efflux from the vesicle. The average lag time that has been found in [19] is about 24 s, whereas, using a different observable (fluctuations with respect to the intensity of the labeled peptide) we observed a lag time of about 100 s. Accordingly, the main source for the fluctuations that we observe could be related to the leaflet asymmetry in the peptide concentration whereas pore formation is highly favored when the peptide is distributed in the two bilayer leaflets. On the basis of our data we cannot obtain any evidence about the mechanistic process that eventually leads to the decrease of the pore diameter.

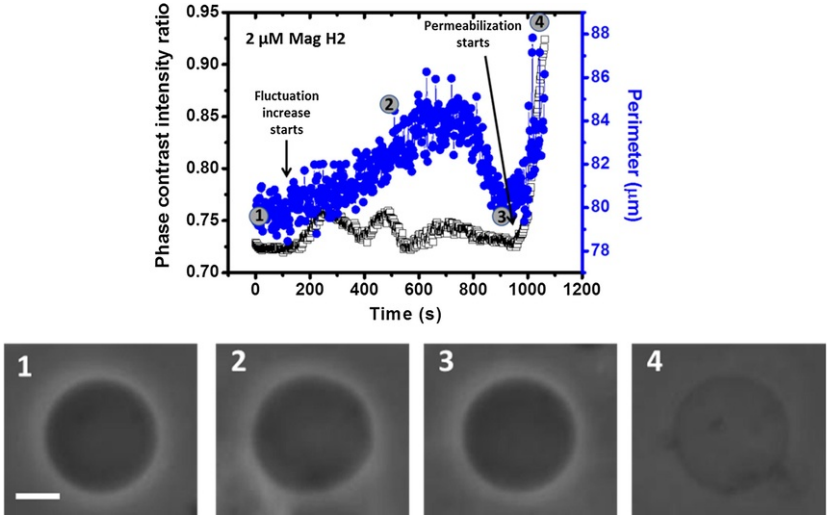

Fig. 7 Variation of the phase contrast and the perimeter value measured at the equatorial plane of a POPC GUV as it interacts with a 2 µM Mag H2 concentration. Hollow squares represent the phase contrast intensity ratio obtained by considering the average intensity of a region external to the vesicle and the average contrast value inside the vesicle. The blue circles represent the approximate value of the perimeter of the vesicle at the equatorial plane as an observable used to report lipid bilayer fluctuations. The phase contrast images of the vesicle reporte below have been obtained at the instants numbered in the plot (bar = 10 µm). (For interpretation of the references to colour in this figure legend, the reader is referred to the web version of this article.)

3.6 Effect of Mag H2 on the lipid bilayer bending constant

In MAT experiments, the vesicle projection inside the pipette is a sort of amplification of the lipid bilayer area changes. However, in the MAT set-up, changes in the bending constant of the lipid bilayer could produce a variation of the apparent vesicle area. Accordingly, we decided to study the changes of the bending constant of lipid bilayers due to the adsorption of the peptides by flickering spectroscopy. The effect of AMPs on lipid bilayer fluctuations has already been studied by flickering microscopy [60,61] establishing for example in the case of Mag 2 a strong effect, in particular a decrease, on the bending constant of POPC membranes [26]. Table 2 shows the effects of low Mag H2 concentrations (0.25–0.3 µM) on the bending constant of DOPC and POPC bilayers. The low concentration of Mag H2 assures that the permeabilization processes is not obtained. This is necessary because the permeabilization typically produces an increase of the vesicle volume producing a tensed bilayer for which the fluctuations are difficult to be measured. Fig. 8 shows an example of the procedure used to identify the vesicle contour (see Par S6 for the details and Movie S7 for the complete contour reconstruction) and the comparison between a pure POPC vesicle and a POPC vesicle exposed to a 0.3 µM Mag H2 solution. The results show that Mag H2 decreases the bending constant of the bilayer, with a similar effect for both DOPC and POPC. This effect could be related to a decrease of the bilayer thickness as has been detected for Mag H2 [62,63].

Table 2 Bending constant values for POPC and DOPC vesicles measured by flickering spectroscopy before and after the exposure to low Mag H2 concentrations (before producing the permeabilization effect).

	Control	Mag H2[C]
POPC	**(26 ± 6) k_BT** (n = 3)	**(11 ± 2) k_BT 0.25 µM** (n = 7)

DOPC	**(21 ± 2) k_BT** (n = 7)	**(7 ± 2) k_BT 0.3 µM** (n = 17)

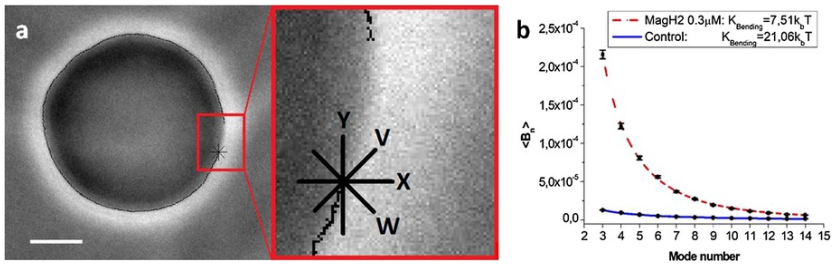

Fig. 8 (a) Image of a DOPC GUV exposed to 0.30 µM Mag H2. Part of the GUV contour is zoomed in order to show the different directions used for gradient of pixels evaluation. Scale bar = 10 µm; (b) fit of experimental n> coefficients obtained from a fluctuating POPC GUV observed at room temperature (22C°) in control condition (continuous blue line), and exposed to Mag H2 0.3 µM (dashed red line). (For interpretation of the references to colour in this figure legend, the reader is referred to the web version of this article.)

4 Conclusion

In this work, we studied, by exploiting GUVs, the permeabilization activity of Mag H2, a peptide obtained by changing 5 residues to the natural antimicrobial peptide Mag 2. Mag H2 is endowed with increased hydrophobicity with respect to Mag 2 and, to the best of our knowledge, no previous studies used GUVs and the related optical microscopy approaches to study the activity of this peptide. The aim of the study was to shed light on the mechanism of action of Mag H2 compared to the well-studied mechanism of Mag 2 with particular emphasis on figuring out of the role played by the enhanced hydrophobicity on the poration mechanism. In fact, together with the different selectivity which is associated to the increased hydrophobicity it is possible that the different physical and chemical properties of the peptides could give rise to different mechanism for the permeabilization activity. We found that Mag H2 has a strong activity also on zwitterionic bilayers and the presence of negatively charged lipids such as PG has a protective effect on the permeabilization activity at variance with the natural Mag 2. We associated this behavior to an increased role of the monolayer curvature in the pore formation mechanism, probably due to deeper penetration of Mag H2 in the hydrophobic region of the bilayer. Accordingly, the increased hydrophobicity of peptides could make the intrinsic monolayer curvature aspects more relevant than the electrostatic effects. In the future, detailed experiments as a function of temperature could shed new light on this aspect. In fact, the intrinsic monolayer curvature can be modulated by temperature and the tendency to form toroidal pores could be consequently affected. Concerning the mechanism of pore formation, our results can be interpreted as consistent with the formation of a toroidal structure and the sequence of steps leading to the permeabilization that we observed are consistent with what has been obtained in other previous studies for Mag 2 [19]. In particular, it seems that pore formation occurs only after the peptide has translocated to the internal leaflet of the GUV, The results we obtained are in agreement with the MD simulation studies in which the formation of disordered toroidal pores has been obtained in the specific case of Mag H2 in PC lipid bilayers [30]. It could be interesting to extend the simulation studies to the case of PG lipids to investigate in more details the role of lipid curvature with respect to electrostatic effects.

Appendix A. Supplementary material

Supplementary data to this article can be found online at https://doi.org/10.1016/j.jcis.2019.06.028.

Supplementary video 1

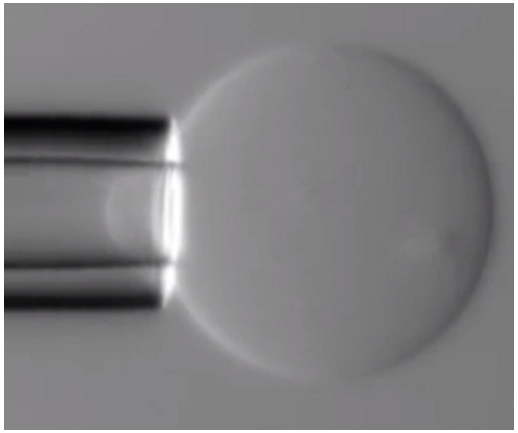

Supplementary video 2

Supplementary video 3

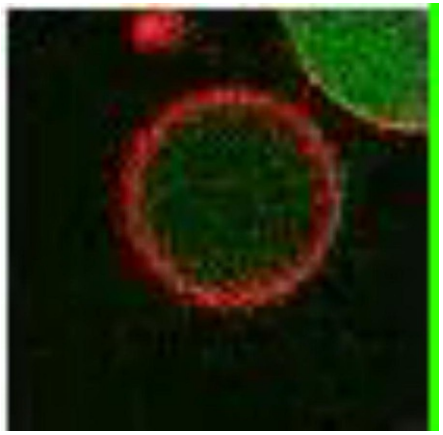

Supplementary video 4

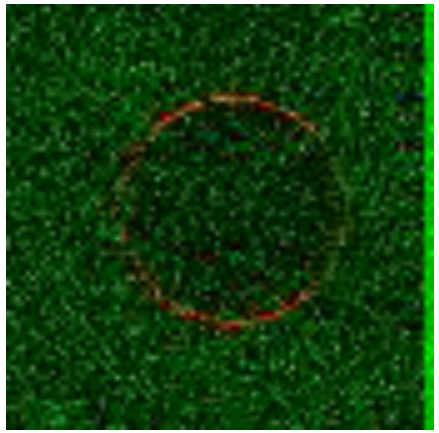

Supplementary video 5

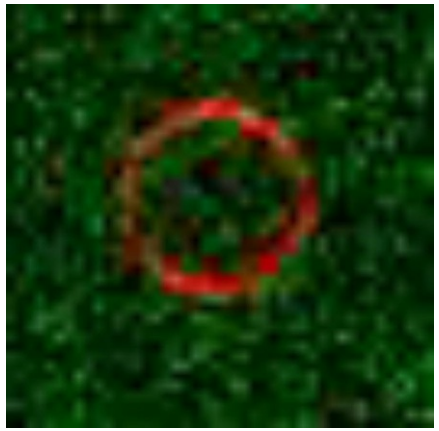

Supplementary video 6

Supplementary video 7

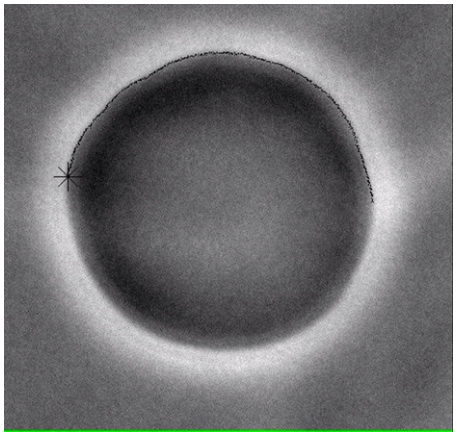

References

[1] K. Mølbak, Spread of resistant bacteria and resistance genes from animals to humans - the public health consequences, *J. Vet. Med. Ser. B Infect. Dis. Vet. Public Heal.* **51**, 2004, 364–369, https://doi.org/10.1111/j.1439-0450.2004.00788.x.

[2] D.I. Andersson, D. Hughes and J.Z. Kubicek-Sutherland, Mechanisms and consequences of bacterial resistance to antimicrobial peptides, *Drug Resist. Updat.* **26**, 2016, 43–57, https://doi.org/10.1016/j.drup.2016.04.002.

[3] J.O'. Neill, Antimicrobial resistance: tackling a crisis for the health and wealth of nations the review on antimicrobial resistance chaired, *HM Gov. Wellcome Trust.* 2014, 1–20, https://doi.org/10.1038/510015a.

[4] E.Y. Furuya and F.D. Lowy, Antimicrobial-resistant bacteria in the community setting, *Nat. Rev. Microbiol.* **4**, 2006, 36–45, https://doi.org/10.1038/nrmicro1325.

[5] World Health Organization, ed., Antimicrobial resistance: global report on surveillance, World Health Organization, Geneva, Switzerland, 2014.

[6] A. Giuliani, G. Pirri and S.F. Nicoletto, Antimicrobial peptides: an overview of a promising class of therapeutics, *Cent. Eur. J. Biol.* **2**, 2007, 1–33.

[7] W. Aoki and M. Ueda, Characterization of antimicrobial peptides toward the development of novel antibiotics, *Pharmaceuticals* **6**, 2013, 1055–1081.

[8] M. Zasloff, Antimicrobial peptides of multicellular organisms, *Nature* **415**, 2002, 389–395, https://doi.org/10.1038/415389a.

[9] T. Koprivnjak and A. Peschel, Bacterial resistance mechanisms against host defense peptides, *Cell. Mol. Life Sci.* **68**, 2011, 2243–2254, https://doi.org/10.1007/s00018-011-0716-4.

[10] K.A. Brogden, Antimicrobial peptides: pore formers or metabolic inhibitors in bacteria?, *Nat. Rev. Microbiol.* **3**, 2005, 238–250, https://doi.org/10.1038/nrmicro1098.

[11] L.T. Nguyen, E.F. Haney and H.J. Vogel, The expanding scope of antimicrobial peptide structures and their modes of action, *Trends Biotechnol.* **29**, 2011, 464–472, https://doi.org/10.1016/j.tibtech.2011.05.001.

[12] A. Pokorny, T.H. Birkbeck and P.F.F. Almeida, Mechanism and kinetics of δ-lysin interaction with phospholipid vesicles, *Biochemistry* **41**, 2002, 11044–11056, https://doi.org/10.1021/bi020244r.

[13] R.F. Epand, W.L. Maloy, A. Ramamoorthy and R.M. Epand, Probing the "charge cluster mechanism" in amphipathic helical cationic antimicrobial peptides, *Biochemistry* **49**, 2010, 4076–4084.

[14] W.C. Wimley, Describing the mechanism of antimicrobial peptide action with the interfacial activity model, *ACS Chem. Biol* **5**, 2010, 905–917, https://doi.org/10.1021/cb1001558.

[15] D.W. Hoskin and A. Ramamoorthy, Studies on anticancer activities of antimicrobial peptides, *Biochim. Biophys. Acta (BBA)-Biomembranes* **1778**, 2008, 357–375.

[16] H.W. Huang and N.E. Charron, Understanding membrane-active antimicrobial peptides, *Q. Rev. Biophys.* **50**, 2017, 1–13, https://doi.org/10.1017/S0033583517000087.

[17] P.F. Almeida and A. Pokorny, Mechanisms of antimicrobial, cytolytic, and cell-penetrating peptides: from kinetics to thermodynamics, *Biochemistry* **48**, 2009, 8083–8093, https://doi.org/10.1021/bi900914g.

[18] M.Z. Islam, J.M. Alam, Y. Tamba, M.A.S. Karal and M. Yamazaki, The single GUV method for revealing the functions of antimicrobial, pore-forming toxin, and cell-penetrating peptides or proteins, *Phys. Chem. Chem. Phys.* **16**, 2014, 15752–15767, https://doi.org/10.1039/c4cp00717d.

[19] M.A.S. Karal, J.M. Alam, T. Takahashi, V. Levadny and M. Yamazaki, Stretch-activated pore of the antimicrobial peptide, magainin 2, *Langmuir* **31**, 2015, 3391–3401, https://doi.org/10.1021/la503318z.

[20] E. Evans and D. Needham, Physical properties of surfactant bilayer membranes: thermal transitions, *Elasticity, Rigidity, Cohesion, Colloid. Interact.* **2**, 1987, 4219–4228.

[21] E. Evans and W. Rawicz, Entropy-driven tension and bending elasticity in condensed-fluid membranes, *Phys. Rev. Lett.* **64**, 1990, 2094–2097, https://doi.org/10.1103/PhysRevLett. 64.2094.

[22] K. Olbrich, W. Rawicz, D. Needham and E. Evans, Water permeability and mechanical strength of polyunsaturated lipid bilayers, *Biophys. J.* **79**, 2000, 321–327, https://doi.org/10.1016/S0006-3495(00)76294-1.

[23] Y. Sun, C.C. Lee, W.C. Hung, F.Y. Chen, M.T. Lee and H.W. Huang, The bound states of amphipathic drugs in lipid bilayers: Study of curcumin, *Biophys. J.* **95**, 2008, 2318–2324, https://doi.org/10.1529/biophysj.108.133736.

[24] R. Kwok and E. Evans, Thermoelasticity of large lecithin bilayer vesicles, *Biophys. J.* **35**, 1981, 637–652, https://doi.org/10.1016/S0006-3495(81)84817-5.

[25] Y. Sun, W.C. Hung, F.Y. Chen, C.C. Lee and H.W. Huang, Interaction of tea catechin (-)-epigallocatechin gallate with lipid bilayers, *Biophys. J.* **96**, 2009, 1026–1035, https://doi.org/10.1016/j.bpj.2008.11.007.

[26] H. Bouvrais, P. Méléard, T. Pott, K.J. Jensen, J. Brask and J.H. Ipsen, Softening of POPC membranes by magainin, *Biophys. Chem.* **137**, 2008, 7–12, https://doi.org/10.1016/j.bpc.2008.06.004.

[27] M.Z. Islam, S. Sharmin, V. Levadnyy, S.U. Alam Shibly and M. Yamazaki, Effects of mechanical properties of lipid bilayers on the entry of cell-penetrating peptides into single vesicles, *Langmuir* **33**, 2017, 2433–2443, https://doi.org/10.1021/acs.langmuir.6b03111.

[28] S. Arasteh and M. Bagheri, Molecular dynamics simulation and analysis of the antimicrobial peptide-lipid bilayer interactions, *In Antimicrob. Pept.* 2017, 103–118, https://doi.org/10.1007/978-1-4939-6737-7_8.

[29] P. La Rocca, P.C. Biggin, D.P. Tieleman, M.S.P. Sansom, Simulation-studies-of-the-interaction-of-antimicrobial-peptides-and-lipid-bilayers_1999_Biochimica-et-Biophysica-Acta-BBA-Biomembranes.pdf 1462 (1999) 185–200.

[30] H. Leontiadou, A.E. Mark and S.J. Marrink, Antimicrobial peptides in action, *J. Am. Chem. Soc.* **128**, 2006, 12156–12161, https://doi.org/10.1021/ja062927q.

[31] M. Zasloff, Magainins, a class of antimicrobial peptides from *Xenopus* skin: isolation, characterization of two active forms, and partial cDNA sequence of a precursor, *Proc. Natl. Acad. Sci.* **84**, 1987, 5449–5453.

[32] K. Matsuzaki, K.I. Sugishita, M. Harada, N. Fujii and K. Miyajima, Interactions of an antimicrobial peptide, magainin 2, with outer and inner membranes of Gram-negative bacteria, *Biochim. Biophys. Acta - Biomembr.* **1327**, 1997, 119–130, https://doi.org/10.1016/S0005-2736(97)00051-5.

[33] S.J. Ludtke, K. He, W.T. Heller, T.A. Harroun, L. Yang and H.W. Huang, Membrane pores induced by magainin, *Biochemistry* **35**, 1996, 13723–13728, https://doi.org/10.1021/bi9620621.

[34] L. Yang, T.M. Weiss, R.I. Lehrer and H.W. Huang, Crystallization of antimicrobial pores in membranes: magainin and protegrin, *Biophys. J.* **79**, 2000, 2002–2009, https://doi.org/10.1016/S0006-3495(00)76448-4.

[35] T. Tachi, R.F. Epand, R.M. Epand and K. Matsuzaki, Position-dependent hydrophobicity of the antimicrobial magainin peptide affects the mode of peptide-lipid interactions and selective toxicity, *Biochemistry* **41**, 2002, 10723–10731, https://doi.org/10.1021/bi0256983.

[36] A.J. Rzepiela, D. Sengupta, N. Goga and S.J. Marrink, Membrane poration by antimicrobial peptides combining atomistic and coarse-grained descriptions, *Faraday Discuss.* **144**, 2010, 431–443, https://doi.org/10.1039/B901615E.

[37] A. Goliaei, K.P. Santo and M.L. Berkowitz, Local pressure changes in lipid bilayers due to adsorption of melittin and magainin-h2 antimicrobial peptides: results from computer simulations, *J. Phys. Chem. B* **118**, 2014, 12673–12679, https://doi.org/10.1021/jp507919p.

[38] A. Pino-Angeles, J.M. Leveritt and T. Lazaridis, Pore structure and synergy in antimicrobial peptides of the magainin family, *PLoS Comput. Biol.* **12**, 2016, 1–17, https://doi.org/10.1371/journal.pcbi.1004570.

[39] D.S. Dimitrov and M.I. Angelova, Lipid swelling and liposome formation mediated by electric fields, *J. Electroanal. Chem. Interfacial Electrochem.* **253**, 1988, 323–336, https://doi.org/10.1016/0022-0728(88)87069-4.

[40] M.-T. Lee, W.-C. Hung, F.-Y. Chen and H.W. Huang, Mechanism and kinetics of pore formation in membranes by water-soluble amphipathic peptides, *Proc. Natl. Acad. Sci.* **105**, 2008, 5087–5092, https://doi.org/10.1073/pnas.0710625105.

[41] J. Pécréaux, H.G. Döbereiner, J. Prost, J.F. Joanny and P. Bassereau, Refined contour analysis of giant unilamellar vesicles, *Eur. Phys. J. E.* **13**, 2004, 277–290, https://doi.org/10.1140/epje/i2004-10001-9.

[42] W.S. Rasband, ImageJ, U. S. National Institutes of Health, Bethesda, Maryland, USA, 1997-2018, (2018) 2018. 1997-2018. <https://imagej.nih.gov/ij/>, <https://imagej.nih.gov/ij/>.

[43] M.J. Sarmento, M. Prieto and F. Fernandes, Reorganization of lipid domain distribution in giant unilamellar vesicles upon immobilization with different membrane tethers, *Biochim. Biophys. Acta - Biomembr.* **2012**, 1818, 2605–2615, https://doi.org/10.1016/j.bbamem.2012.05.028.

[44] P. Schön, A.J. García-Sáez, P. Malovrh, K. Bacia, G. Anderluh and P. Schwille, Equinatoxin II permeabilizing activity depends on the presence of sphingomyelin and lipid phase coexistence, *Biophys. J.* **95**, 2008, 691–698, https://doi.org/10.1529/biophysj.108.129981.

[45] N.B. Leite, A. Aufderhorst-Roberts, M.S. Palma, S.D. Connell, J.R. Neto and P.A. Beales, PE and PS lipids synergistically enhance membrane poration by a peptide with anticancer properties, *Biophys. J.* **109**, 2015, 936–947, https://doi.org/10.1016/j.bpj.2015.07.033.

[46] Y. Tamba and M. Yamazaki, Magainin 2-induced pore formation in the lipid membranes depends on its concentration in the membrane interface, *J. Phys. Chem. B.* **113**, 2009, 4846–4852, https://doi.org/10.1021/jp8109622.

[47] B. Kollmitzer, P. Heftberger, M. Rappolt and G. Pabst, Monolayer spontaneous curvature of raft-forming membrane lipids, *Soft Matter.* **9**, 2013, 10877, https://doi.org/10.1039/c3sm51829a.

[48] K. Matsuzaki, K.I. Sugishita, N. Ishibe, M. Ueha, S. Nakata, K. Miyajima, et al., Relationship of membrane curvature to the formation of pores by magainin 2, *Biochemistry* **37**, 1998, 11856–11863, https://doi.org/10.1021/bi980539y.

[49] D. Bhattacharyya, M. Kim, K.H. Mroue, M. Park, A. Tiwari, M. Saleem, et al., Role of non-electrostatic forces in antimicrobial potency of a dengue-virus derived fusion peptide VG16KRKP: Mechanistic insight into the interfacial peptide-lipid interactions, *Biochim. Biophys. Acta - Biomembr.* **2019**, 1861, 798–809, https://doi.org/10.1016/j.bbamem.2019.01.011.

[50] S.H. Alley, O. Ces, M. Barahona and R.H. Templer, X-ray diffraction measurement of the monolayer spontaneous curvature of dioleoylphosphatidylglycerol, *Chem. Phys. Lipids.* **154**, 2008, 64–67, https://doi.org/10.1016/j.chemphyslip.2008.03.007.

[51] E.E. Ambroggio, F. Separovic, J.H. Bowie, G.D. Fidelio and L.A. Bagatolli, Direct visualization of membrane leakage induced by the antibiotic peptides: maculatin, citropin, and aurein, *Biophys. J.* **89**, 2005, 1874–1881, https://doi.org/10.1529/biophysj.105.066589.

[52] E. Glukhov, M. Stark, L.L. Burrows and C.M. Deber, Basis for selectivity of cationic antimicrobial peptides for bacterial versus mammalian membranes, *J. Biol. Chem.* **280**, 2005, 33960–33967, https://doi.org/10.1074/jbc.M507042200.

[53] A.J. McHenry, M.F.M. Sciacca, J.R. Brender and A. Ramamoorthy, Does cholesterol suppress the antimicrobial peptide induced disruption of lipid raft containing membranes?, *Biochim. Biophys. Acta - Biomembr.* **2012**, 1818, 3019–3024, https://doi.org/10.1016/j.bbamem.2012.07.021.

[54] L.R. Arriaga, I. López-Montero, F. Monroy, G. Orts-Gil, B. Farago and T. Hellweg, Stiffening effect of cholesterol on disordered lipid phases: a combined neutron spin echo + dynamic light scattering analysis of the bending elasticity of large unilamellar vesicles, *Biophys. J.* **96**, 2009, 3629–3637, https://doi.org/10.1016/j.bpj.2009.01.045.

[55] K.A. Riske, Optical Microscopy of Giant Vesicles as a Tool to Reveal the Mechanism of Action of Antimicrobial Peptides and the Specific Case of Gomesin, 1st ed., 2015, Elsevier Inc., 10.1016/bs.adplan.2014.12.001.

[56] E.F. Haney, S. Nathoo, H.J. Vogel and E.J. Prenner, Induction of non-lamellar lipid phases by antimicrobial peptides: a potential link to mode of action, *Chem. Phys. Lipids.* **163**, 2010, 82–93, https://doi.org/10.1016/j.chemphyslip.2009.09.002.

[57] Y. Tamba, H. Ariyama, V. Levadny and M. Yamazaki, Kinetic pathway of antimicrobial peptide magainin 2-induced pore formation in lipid membranes, *J. Phys. Chem. B* **114**, 2010, 12018–12026, https://doi.org/10.1021/jp104527y.

[58] Y. Tamba and M. Yamazaki, Single giant unilamellar vesicle method reveals effect of antimicrobial peptide magainin 2 on membrane permeability, *Biochemistry* **44**, 2005, 15823–15833, https://doi.org/10.1021/bi051684w.

[59] M. Sacchi, D. Balleza, G. Vena, G. Puia, P. Facci and A. Alessandrini, Effect of neurosteroids on a model lipid bilayer including cholesterol: an atomic force microscopy study, *Biochim. Biophys. Acta - Biomembr.* **2015**, 1848, 1258–1267, https://doi.org/10.1016/j.bbamem.2015.01.002.

[60] T. Pott, C. Gerbeaud, N. Barbier and P. Méléard, Melittin modifies bending elasticity in an unexpected way, *Chem. Phys. Lipids.* **185**, 2015, 99–108, https://doi.org/10.1016/j.chemphyslip.2014.05.004.

[61] V. Vitkova, P. Méléard, T. Pott and I. Bivas, Alamethicin influence on the membrane bending elasticity, *Eur. Biophys. J.* **35**, 2006, 281–286, https://doi.org/10.1007/s00249-005-0019-5.

[62] N. Marín-Medina, A. Mescola and A. Alessandrini, Effects of the peptide magainin H2 on supported lipid bilayers studied by different biophysical techniques, *Biochim. Biophys. Acta - Biomembr.* **2018**, 1860, 2635–2643, https://doi.org/10.1016/j.bbamem.2018.10.003.

[63] S. Ludtke, K. He and H. Huang, Membrane thinning caused by magainin 2, *Biochemistry* **34**, 1995, 16764–16769, https://doi.org/10.1021/bi00051a026.

Appendix A. Supplementary material

The following are the Supplementary data to this article:

Multimedia Component 1 

Supplementary video 1

Multimedia Component 2 

Supplementary video 2

Multimedia Component 3 

Supplementary video 3

Multimedia Component 4 

Supplementary video 4

Multimedia Component 5 

Supplementary video 5

Multimedia Component 6 

Supplementary video 6

Multimedia Component 7 

Supplementary video 7

Multimedia Component 8

Supplementary data 8

Graphical abstract

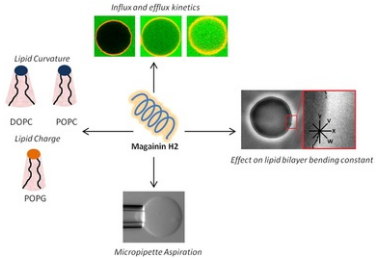

Queries and Answers

Query: Your article is registered as a regular item and is being processed for inclusion in a regular issue of the journal. If this is NOT correct and your article belongs to a Special Issue/Collection please contact r.saravanakumar@elsevier.com immediately prior to returning your corrections.
Answer: Yes

Query: The author names have been tagged as given names and surnames (surnames are highlighted in teal color). Please confirm if they have been identified correctly.
Answer: Yes

Query: To maintain sequential order, Eq. [1] has been changed to Eq. [3]. Please check, and correct if necessary.
Answer: Ok

Query: Correctly acknowledging the primary funders and grant IDs of your research is important to ensure compliance with funder policies. We could not find any acknowledgement of funding sources in your text. Is this correct? /
Answer: Yes

Query: Please note that as the reference [30] supplied more than once, the repletion has been removed from the list. Please check, and amend accordingly.
Answer: Yes, ref [30] was wrongly mentioned twice; Now it is Ok